Well-Defined All-Conducting Block Copolymer Bilayer Hybrid Nanostructure: Selective Positioning of Lithium Ions and Efficient Charge Collection

In Young Song,† Young Soo Kwon,† Jongchul Lim, and Taiho Park*

Department of Chemical Engineering, Pohang University of Science and Technology, San31, Nam-gu, Pohang, Kyungbuk 790-784, Korea. †These authors share equal contribution.

ABSTRACT A block copolymerization of nonfunctionalized conducting monomers was developed to enable the successful synthesis of a highly insoluble 3,4-(ethylenedioxy)thienyl-based all-conducting block copolymer (PEDOT-*b*-PEDOT-TB) that could encapsulate nanocrystalline dyed TiO_2 particles, resulting in the formation of an all-conducting block copolymer bilayer hybrid nanostructure (TiO_2/Dye/PEDOT-*b*-PEDOT-TB). Lithium ions were selectively positioned on the outer PEDOT-TB surface. The distances through which the positively charged dye and PEDOT-TB(Li^+) interacted physically or through which the TiO_2 electrode and the Li^+ centers on PEDOT-TB(Li^+) interacted ionically were precisely tuned and optimized within *ca.* 1 nm by controlling the thickness of the PEDOT blocking layer (the block length). The optimized structure provided efficient charge collection in an iodine-free dye-sensitized solar cell (DSC) due to negligible recombination of photoinduced electrons with cationic species and rapid charge transport, which improved the photovoltaic performance (η = 2.1 → 6.5%).

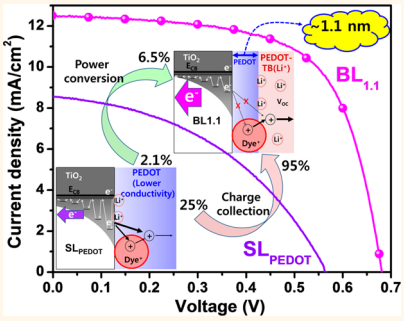

KEYWORDS: all-conducting block copolymer · bilayer nanostructure · photoelectrochemical polymerization · selective positioning of lithium ions

The properties of interfaces between organic and inorganic materials in heterojunctions are relevant to a variety of electronic applications.[1−7] The performances of such devices strongly depend on the kinetics of the charge transfer reactions and the thermodynamic properties (*e.g.*, energetic difference at the junctions) at the heterogeneous interfaces.[8,9] Heterogeneous interfaces, especially in iodine-free dye-sensitized solar cells (DSCs),[10] can be controlled by modifying the interfacial properties to improve the photovoltaic performance. After electron injection into the conduction band (CB) from a dye excited by photon absorption, an electron relaxes to the lowest energy level of the CB and is subsequently trapped in the intraband states (Figure S1 illustrates the mechanism in detail).[11,12] Trapping then increases the electron collection time (τ_{coll}) through the TiO_2 particles. The photoinduced electrons [$e^-(TiO_2)$] in the trap states can recombine with dye cations (Dye^+, at a rate of R_{Dye+})[13] or the cationic hole transporting material (HTM^+, at a rate of R_{HTM+}) (Figure 1a).[14] These recombination reactions are rapid (the characteristic electron recombination time, τ_{rec}, is short) if many trap states in the lower-lying quasi-Fermi level of the TiO_2 electrode exist. The R_{HTM+} value is crucial to the photovoltaic performance of a DSC containing organic cationic HTMs. R_{HTM+} may be slowed (τ_{rec} may be longer) if hole transport to the counter electrode through a HTM layer with a higher conductivity is rapid.

Heterogeneous interfaces, including nanocrystalline TiO_2 electrodes and the HTM layer, have been modified using 4-*tert*-butylpyridine (*t*BP),[15,16] lithium ions,[3,17] or their mixtures.[18,19] For example, Boschloo *et al.*[20] and others[21,22] demonstrated that increasing the occupancy of the trap states by adding *t*BP, which deprotonates the TiO_2 surface, reduced R_{HTM+} and R_{Dye+} and increased the open circuit voltage (V_{OC}) by suppressing the dark current. The theoretical V_{OC} is determined by the energy difference between the quasi-Fermi level of a

* Address correspondence to taihopark@postech.ac.kr.

Received for review March 23, 2014 and accepted June 10, 2014.

Published online June 10, 2014
10.1021/nn5016083

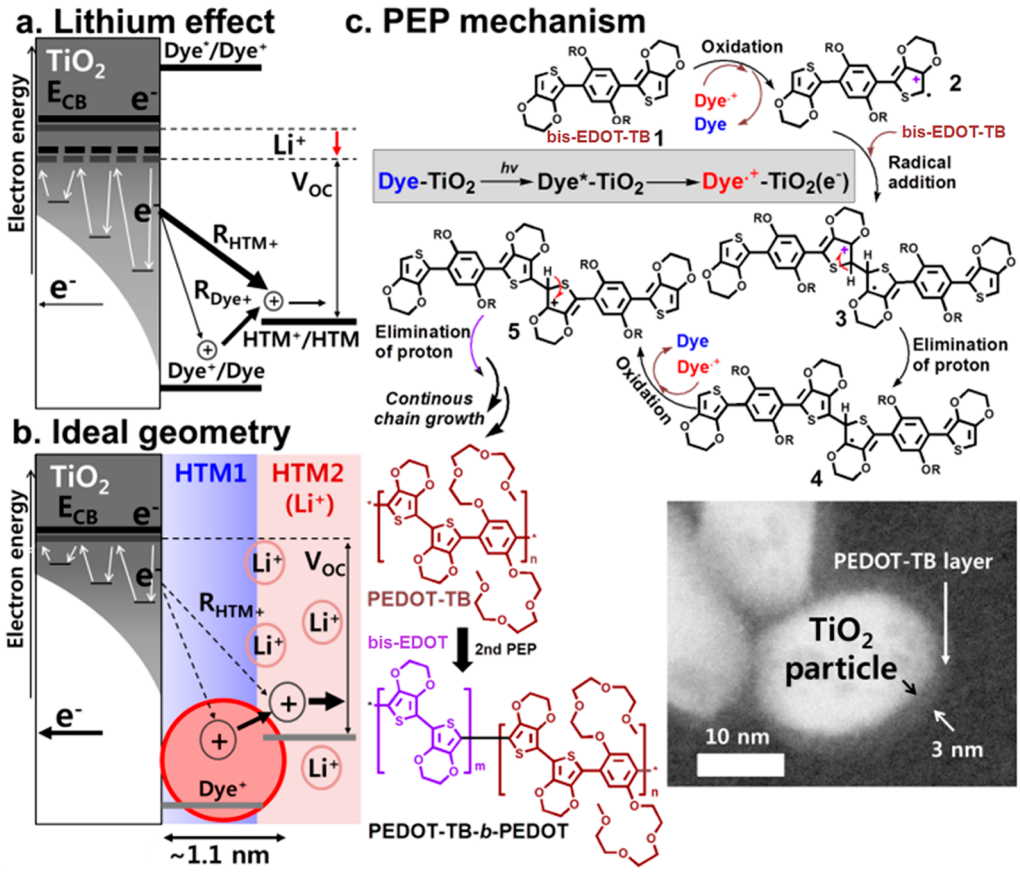

Figure 1. (a) Lithium effects at the dye/TiO_2/HTM interface. (b) Ideal geometry for a DSC. (c) *In situ* PEP mechanism. Inset: TEM image of TiO_2 particles encapsulated with PEDOT-TB.

nanocrystalline TiO_2 electrode under illumination and the redox level of the HTM. Meyer *et al.*[23] and others[24,25] reported that the addition of Li^+ to an aprotic electrolyte shifted the band edge away from the vacuum level (producing lower-lying quasi-Fermi levels in the TiO_2 electrode) due to the adsorption of Li^+ on the polar surfaces of the TiO_2 particles. This effect increased the rate of interfacial charge injection; however, V_{OC} decreased and R_{Dye+} and R_{HTM+} increased (Figure 1a). Snaith *et al.*, Durrant *et al.*, and Yanagida *et al.* independently demonstrated that Li^+ increased the hole transport properties in an organic matrix and improved the fill factor (*FF*) (Figure S2).[26−28]

In view of these results, we sought to optimize the structure of an iodine-free DSC having an HTM bilayer structure (HTM1 and HTM2(Li^+)) (Figure 1b). The confinement of Li^+ ions to the outer HTM2(Li^+) layers avoids the introduction of lower-lying quasi-Fermi levels into the TiO_2 electrode. The selective positioning of Li^+ on the HTM2(Li^+) layer was expected to simultaneously maintain a high V_{OC}, slow R_{Dye+} and R_{HTM+}, and speed hole transport. The physical contact distance between the HTM2(Li^+) layer and the Dye^+ could be tuned according to the thickness of the HTM1 layer to optimize hole transport from the HTM2(Li^+)−Dye^+ regeneration reaction on a time scale shorter than R_{HTM+}. This ideal structure may provide significant improvements in photovoltaic devices.

Recently, we successfully demonstrated photoelectrochemical polymerization (PEP)[29] using a novel small molecule, bis-EDOT-TB (1,4-bis[2-(3,4-ethylenedioxy)-thienyl]-2,5-bis{2-[2-(2-methoxyethoxy)ethoxy]ethoxy}-benzene), having tetraethylene glycol (TEG) side chains for chelating Li^+ ions with a binding constant of K = 495 M^{-1} in acetonitrile.[29] We carefully investigated the PEP mechanisms and found that the polymerization only occurred at sites neighboring the dye moieties; thus, the sequential polymerization of two monomers produced a well-defined conducting block copolymer (Figure 1c). Previously, several groups,[30,31] including ourselves,[32] reported the synthesis of a set of all-conducting block copolymers prepared *via* a quasi-living Grignard metathesis (GRIM) of functional monomers[33,34] or *via* a coupling reaction involving two monofunctionalized polymers.[35,36] To the best of our knowledge, the synthesis of highly insoluble all-conducting block copolymers by a PEP method employing nonfunctionalized monomers has not previously been reported, probably due to the presence of uncontrollable active sites.[37] Herein, we report a novel synthesis of well-defined conducting block copolymers, which are formed on the surfaces of nanocrystalline TiO_2

particles. This approach permitted the selective positioning of lithium ions on the PEDOT-TB blocks only and the realization of an ideal device (Figure 1b), thereby affording an improvement in the photovoltaic performances in iodine-free DSCs.

RESULTS AND DISCUSSION

PEP Mechanism. Figure 1c illustrates that PEP of bis-EDOT-TB for PEDOT-TB was performed under illumination with Xe arc lamp (above 520 nm) at 0.2 V of a constant bias. An oxidized dye ($Dye^{\cdot+}$), which is generated by electron injection of an excited dye (Dye*) into the TiO_2 conduction band after a dye (Dye) absorbs light, is neutralized by an electron transfer reaction from bis-EDOT-TB (**1**). This reaction generates radical cation species (**2**) of bis-EDOT-TB which is coupled with another monomer, bis-EDOT-TB, affording a dimer (**3**) with a radical cation. After elimination of proton on **3** for aromatization of one of thiophene units, the resulting radical species (**4**) transfers one electron to a $Dye^{\cdot+}$, generating a cationic dimer (**5**) and a neutralized dye (Dye). An aromatization (**5**) by the elimination reaction of proton on the cationic dimer provides a neutralized species. The continuous catalytic cycle is able to giving a polymer, PEDOT-TB. The polymer might only grow at the neighbors of TiO_2 particles, thus between TiO_2 particles and already grown polymer chains. Replacement of bis-EDOT-TB with the bis-EDOT monomer solutions (see Figure S3 for detailed experiments) after the first PEP reaction of bis-EDOT-TB afforded a block copolymer (see the Scheme S1 for the full mechanism). The neutralization of Dye^+ (**1** → **2** or **4** → **5**) should occur on the surface of TiO_2 particles; thus, the coupling reaction (**2** → **3**) of the radical species with a new monomer for chain growing should also occur at the interface between the surface of TiO_2 particles and the grown chains. The dyed TiO_2 particles were thus encapsulated by PEDOT-TB (see the insets in Figure 1) to produce a 3 nm thick PEDOT-TB layer after 1200 s. A 3 nm thick polymer layer is the thickest functional layer that may be produced using this method, because the incident light is absorbed by thicker polymer layers (Figure S4). This also indicated that the PEP could not generate brush-type polymers from the dye molecules by the initiation at the end further away from the dye molecule (see Figure S5 for illustrated comparison of the PEP and the brush-type polymerization).

Figure 2a shows a representative reaction profile for a PEP involving bis-EDOT-TB monomers, monitored according to the current density as a function of the reaction time. The current density reached a maximum current density at 200 s and then decreased exponentially over time. The integrated area under the current density curve was equivalent to the quantity of charge (*Q*) transferred during the PEP process. Greater *Q* during the PEP reaction increased the polymer chain length or number. Matrix-assisted laser desorption/ionization-time-of-flight mass spectrometry (MALDI-TOF MS)[38] analysis revealed an increase in molecular weight (MW) with the reaction time (see the inset in Figure 2a). It is noticed that we failed to characterize the MW or structure using gel permeation chromatography (GPC), dynamic light scattering (DLS), or ^{1}H NMR techniques due to the insolubility of the polymers in various organic solvents, including water, chloroform, dichlorobenzene, THF, DMF, or DMSO.

Synthesis of the Block Copolymers. Replacement of bis-EDOT-TB with the bis-EDOT monomers after the first PEP reaction of bis-EDOT-TB afforded a bilayer structure with a first PEDOT and a second PEDOT-TB layer in a block copolymer (① → ② in Figure 2b), as chain growth proceeded only at the end of the growing PEDOT-TB strand. The MW after the second PEP reaction exceeded 6800 Da, an increase from 4100 Da (Figure 2c), indicating that the structure consisted of PEDOT-*b*-PEDOT-TB block copolymers (Figure S6) shows the chemical composition determined by Raman spectroscopy. The sequential PEP reaction involving a first rigid monomer (bis-EDOT) followed by larger less rigid monomer (bis-EDOT-TB) did not produce further chain growth (③ → ④ in Figure 2b), demonstrating that the monomers must access the dyes through the already-formed polymer layer to permit chain growth (Figure 2d). One-dimensional X-ray diffraction (1D-XRD) studies at the Pohang Accelerator Laboratory (PAL) revealed the crystalline structures of the polymers, although no distinctive peaks were observed (Figure S7).

Bipolarons were readily generated in the PEDOT-TB layer during the PEP reaction (Figure S8), possibly contributing to the PEP reaction on the outer surface of the PEDOT-TB layer. The second PEP reaction was carried out with bis-EDOT on a first compact PEDOT-TB layer (PEP time: 1200 s); however, no further polymerization reactions on the surface of the first PEDOT-TB layer were observed (Figure S9), indicating that the polarons in the first PEDOT-TB layer did not participate in the PEP reaction. This result confirmed that the monomers needed to access the dyes through the already-formed polymer layer, thereby providing an explanation for why the polymer layer thickness was limited to 3 nm in this study. In turn, the polymerization cannot be initiated at the end further away from the dye molecule.

Characterization of the Block Copolymer Bilayers. The phase-inverted bilayer nanostructure composed of two polymer blocks was characterized by measuring the water contact angles (Θ_{water})[29] on the surfaces of the PEDOT-TB, PEDOT, and polymer bilayers obtained from the sequential PEP reactions employing the first bis-EDOT-TB monomer followed by the second bis-EDOT monomer (Figure 3a). The Θ_{water} of the polymer bilayer was 26.3°, which is very close to that of a

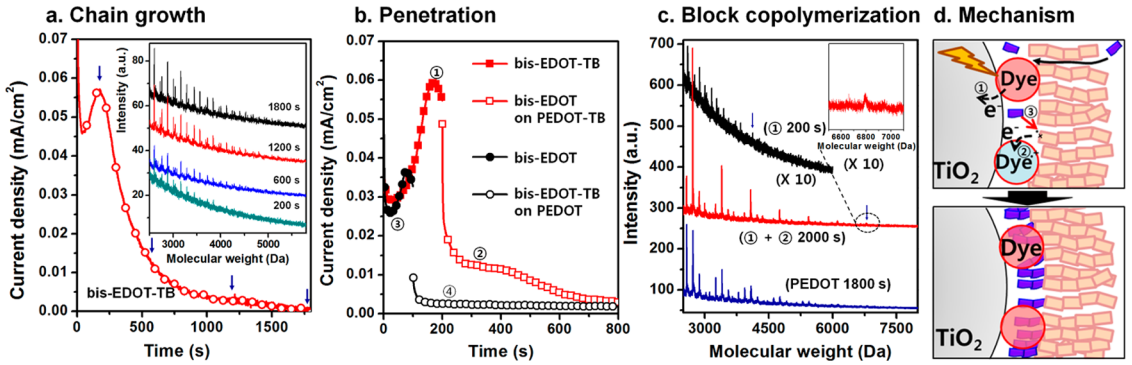

Figure 2. (a) Current−time profiles of the PEP reactions on dyed-TiO_2 in a bis-EDOT-TB solution (10 mM) at a 0.2 V. Inset: MALDI-TOF MS spectra of PEDOT-TB (200−1800 s). (b) Current−time profile of the sequential PEP reactions. (c) MALDI-TOF MS spectra for PEDOT-TB (200 s), a block copolymer (① (200 s) → ② (1800 s)), and PEDOT (1800 s). Inset: Expanded spectra of the block copolymer over the range 6600−7000. (d) Illustration of PEP reaction of bis-EDOT on PEDOT-TB under illumination.

PEDOT-TB layer (22.5°) but much smaller than that of a PEDOT layer (72.4°). This result demonstrated that bis-EDOT was at the sites between the TiO_2 surface and the first PEDOT-TB layer after penetrating the first hydrophilic PEDOT-TB layer.

The bilayer structure was further characterized using secondary ion mass spectroscopy (SIMS) methods (Figure 3b). The most lithium ions should be located at the outer PEDOT-TB layer (Surface), which is only capable of chelating lithium ions. For the detection of lithium ions, the more red color appears when the more lithium ions exist. Indeed, higher concentrations of lithium atoms were only detected in the outer PEDOT-TB layer (see the Figure S10 for the additional SIMS images). In addition, we prepared a block copolymer containing polypyrrole (PPy) (PEDOT-TB-*b*-PPy) to confirm the formation of the bilayer structure. In this case, a pyrrole monomer, rather than a bis-EDOT, was used to differentiate a nitrogen atom from sulfur atoms in the thiophene-based monomers (Figure 3c). In addition, $LiClO_4$ was used in the PEP, instead of LiTFSI containing sulfur atom, which could be detected in the elemental mapping of the resulting polymer. The change of dopants did not contribute to the PEP. Higher concentrations of nitrogen atoms were only detected in the second layer (Figure 3d), whereas higher concentrations of sulfur atoms were observed in the first layer (Figure 3e). These results demonstrated that the second monomer (pyrrole) penetrated the surface of the dyed-TiO_2 particles through the first PEDOT-TB layer. Therefore, the sequential PEP reaction employing the first bis-EDOT-TB followed by second bis-EDOT monomers yielded a bilayer nanostructure with a first PEDOT layer and a second PEDOT-TB layer on the surfaces of the nanocrystalline TiO_2 particles.

Photovoltaic Performances. The selective positioning of Li^+ ions on the bilayer polymeric hybrid nanostructure was examined in the context of an iodine-free DSC in the presence of Li^+TFSI^- and *t*BP, as additives.[30,31] The thickness of the layers composed of PEDOT and PEDOT-TB blocks could be controlled by varying the concentrations (2.5−20 mM) of the bis-EDOT-TB monomer holding the concentration of the bis-EDOT monomer constant (Figure S11). A series of bilayer DSCs were prepared (abbreviated $BL_{1.5}$, $BL_{1.1}$, and $BL_{0.6}$, where the subscripts indicate the thickness of the PEDOT layer). The thickness of each layer was estimated according to the accumulated charge density (Table 1, Table S1 and Figure S12), and the total thickness was found to be close to 3 nm, consistent with the values estimated from the TEM images. As the bis-EDOT-TB concentration increased, the PEDOT-TB layer thickness increased whereas the PEDOT layer thickness decreased (Figure 4a). The device prepared with an ionic liquid only (IL, 1,3-ethylmethylimidazolium trifluoromethylsulfone imide: EmITFSI) did not display photovoltaic properties (Table 2 and Figure 4b). On the other hand, the single layered DSCs (9 μm of TiO_2 layer) prepared with PEDOT and PEDOT-TB (denoted SL_{PEDOT} and $SL_{PEDOT-TB}$, respectively) exhibited 2.1% and 3.1% PCEs, respectively. It is noticed that we previously obtained the best V_{OC} and FF values from the SL_{PEDOT} and $SL_{PEDOT-TB}$ devices having 6 μm thick TiO_2 active layers. As the thickness of the TiO_2 active layer increased, the V_{OC} and FF values decreased due to poor electron collection and significant recombination (see Figure S13 and Table S2). We therefore employed a thicker TiO_2 active layer to demonstrate the bilayer effects on the electron collection and recombination reaction. The bilayer devices ($BL_{1.5}$, $BL_{1.1}$, and $BL_{0.6}$) exhibited dramatic differences in their photovoltaic performances, depending on the thickness of the PEDOT layer (1.5−0.6 nm). The *J*−*V* curves and FF of the $BL_{0.6}$ and $BL_{1.5}$ devices were similar to those of the $SL_{PEDOT-TB}$ and SL_{PEDOT} devices, respectively, even though the photovoltaic performances of the $BL_{0.6}$ and $BL_{1.5}$ devices were better than those of the corresponding single layer devices. Surprisingly, the best performance was obtained from $BL_{1.1}$, with a J_{SC} of 12.5, a V_{OC} of 0.68, a FF of 0.65, and a PCE of 5.5%. The thickness of the PEDOT layer was only 0.5 nm

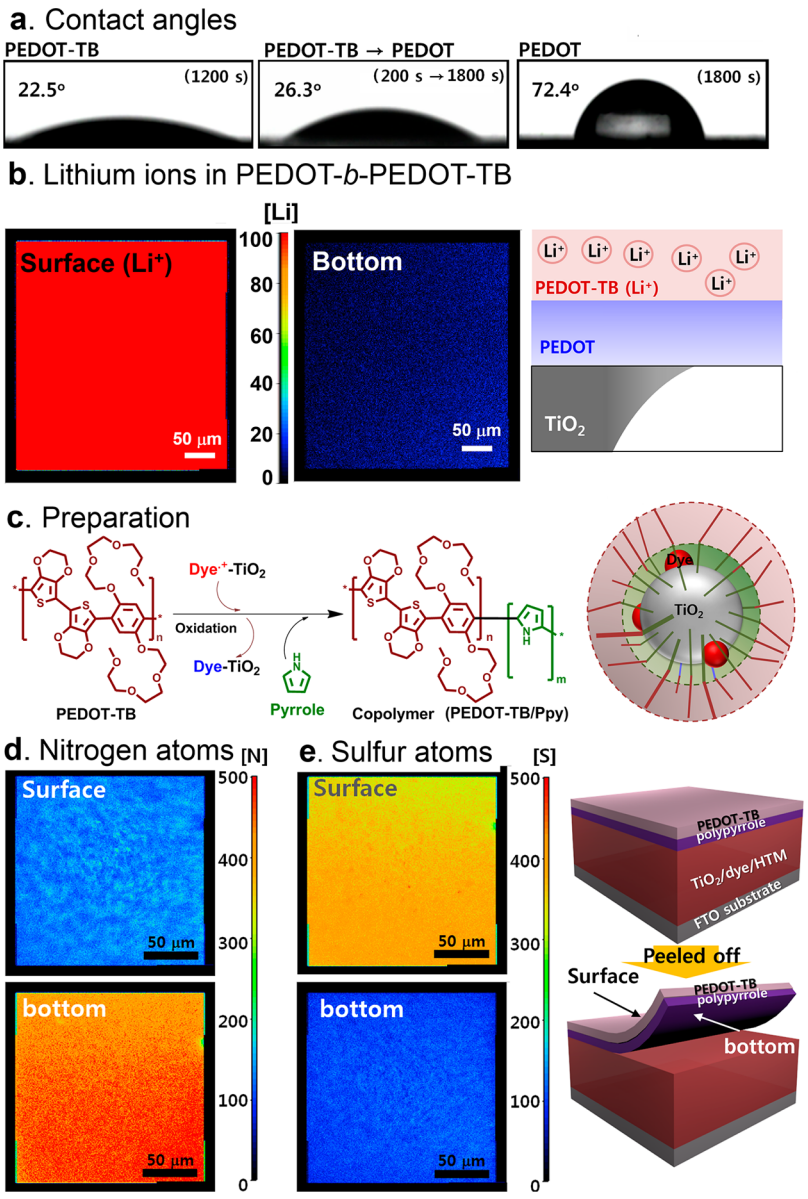

Figure 3. (a) The water contact angles. (b) Lithium ions mapping based on the secondary ion mass spectroscopy (SIMS) measurement at the surface (left) and bottom (right) of the bilayer polymer structure ($BL_{1.1}$). (c) The procedure for preparing an inverted bilayer structure for SIMS measurement. (d and e) Elemental mapping based on SIMS of the nitrogen and sulfur atoms, respectively, at the surface (upper images) or bottom (lower images) of the bilayer polymer structure.

thicker than the layers in the $BL_{0.6}$ and 0.4 nm thinner than the layers in the $BL_{1.5}$ devices.

The dramatic changes in the photovoltaic performances over a 1 nm PEDOT thickness variance were examined by measuring the τ_{coll}, τ_{rec}, and η_{cc} values of the devices (the electron collection time and the recombination time were calculated from the equation: $\tau = 1/2\pi f$, where f is the measured frequency at a minimum point of a Nyquist plot, and the charge collection efficiency was calculated by the equation, $\eta_{cc} = 1 - \tau_{coll}/\tau_{rec}$) based on intensity-modulated photocurrent (IMPS, short-circuit) or photovoltage (IMVS, open-circuit) spectroscopy measurements as shown in Figures S14 and S15.[39] It is noticed that we attempted to measure the quantum yields of the recombination reactions of $e^-(TiO_2)$ with Dye^+ and HTM^+ and the regeneration reaction of Dye^+ with HTM using transient absorption spectroscopy[40,41] and transient mobility spectroscopy,[42] as reported previously; however, these efforts failed due to overlap with the Dye^+ and PEDOT-TB polaron absorption bands. Figure 5a shows the thickness-dependent FFs of the devices. The FF values were reasonably high (0.62−0.65) until the thickness of PEDOT reached 1.1 nm, at which point the values decreased abruptly, reaching 0.47 at 1.5 nm PEDOT thickness. Two factors were considered in rationalizing these results: the physical contact between the PEDOT and PEDOT-TB(Li^+) with the Dye^+, or the conductivity difference between the PEDOT and PEDOT-TB(Li^+). The size of the

sensitizing dye (Z907) on the surfaces of the TiO_2 particles was estimated to be 1.1 nm (Figure S16), and the conductivity (5.2×10^{-7} S/cm) of PEDOT was 1 order of magnitude lower than that (5.3×10^{-6} S/cm) of PEDOT-TB (Figure S17).[29] The PEDOT layer-covered dye molecules apparently facilitated recombination between the holes on PEDOT and the electrons (R_{HTM+}), rather than transferring the holes to the counter electrode through the PEDOT-TB(Li^+) layer (see the inset ($BL_{1.5}$) in Figure 5). This hypothesis was supported by the measurement of shorter τ_{rec} values (Figure 5d) and longer τ_{coll} values in $BL_{1.5}$ (Figure 5e). The J_{SC} values in $BL_{1.5}$ and SL_{PEDOT} were, therefore, reduced (Figure 5b). An inner PEDOT layer thickness of less than 1.0 nm permitted the dye molecules to contact the outer PEDOT-TB(Li^+) layer; thus, hole transport from the Dye^+ moieties to the outer PEDOT-TB(Li^+) layer (*e.g.*, less R_{HTM+}). Interestingly, the J_{SC} value gradually increased to 12.5 ($BL_{1.1}$) from 9.4 mA/cm^2 ($SL_{PEDOT-TB}$). The trend in the J_{SC} values was consistent with that of the τ_{rec} values (Figure 5d) and was mainly determined by the values of R_{Dye+} and R_{HTM+}. The gradual increase in J_{SC} values indicated that the influence of the lithium ions chelated in PEDOT-TB(Li^+) decreased as the PEDOT block layer thickness increased to 1.1 nm (see Figure S18 for an explanation of the roles of the PEDOT block layer). This, in turn, indicated that a 0.6 nm thick PEDOT layer was too thin to neutralize the influence of the lithium ions on the PEDOT-TB(Li^+) layer (see the inset ($BL_{0.6}$) in Figure 5).

The low quasi-Fermi levels of the TiO_2 electrodes in the $SL_{PEDOT-TB}$ and $BL_{0.6}$ devices were reflected in their V_{OC} values (0.53 and 0.56 V, respectively, Figure 5c), which were much smaller than the theoretical V_{OC} value (0.68 V) estimated from the energy difference between the quasi-Fermi level of the TiO_2 electrode and the HOMO level of the HTM. V_{OC} was mainly sensitive to the quasi-Fermi level of the TiO_2 electrode under the experimental conditions, as the HOMO levels of the PEDOT and PEDOT-TB layers were nearly identical (−4.68 eV *vs* vacuum level, Figure S19). The lower V_{OC} value (0.57 V) for the SL_{PEDOT} device was ascribed to both the lower-lying quasi-Fermi level of the TiO_2 electrode upon the adsorption of lithium ions to the

TABLE 1. Charge Transfer/Transport Properties of DSCs

	concentration [mM]		thickness [nm][a]				
	[bis-EDOT-TB]	[bis-EDOT]	$d_{PEDOT-TB}$	d_{PEDOT}	τ_{coll} (ms)[b]	τ_{rec} (ms)[c]	η_{cc}[d]
$SL_{PEDOT-TB}$	10	-	3.2	-	6.11	13.4	0.54
$BL_{0.6}$	20	10	1.8	0.6	4.63	27.8	0.83
$BL_{1.1}$	10	10	1.5	1.1	1.97	41.7	0.95
$BL_{1.5}$	5	10	0.7	1.5	4.63	8.22	0.43
$BL_{1.7}$	2.5	10	0.4	1.7	-	-	-
SL_{PEDOT}	-	10	-	2.7	5.30	7.07	0.25
Optimized	20	10	-	-	-	-	-
IL[g] only	-	-	-	-	-	-	-

[a] See the 12.calculation method. [b] Electron collection time. [c] Electron recombination time. [d] Charge collection efficiency calculated by the equation of $\eta_{cc} = 1 - \tau_{coll}/\tau_{rec}$. [g] Ionic liquid (EmITFSI).

TABLE 2. Photovoltaic Performances and Series/Shunt Resistances of DSCs

	J_{SC} (mA/cm^2)	V_{OC} (V)	FF	PCE (%)[a]	R_s (Ω)	R_{sh} (kΩ)
$SL_{PEDOT-TB}$	9.4	0.53	0.62	3.1	44	8.03
$BL_{0.6}$	11.1	0.56	0.62	3.9	39	8.55
$BL_{1.1}$	12.5	0.68	0.65	5.5	34	14.1
$BL_{1.5}$	8.6	0.65	0.47	2.6	57	3.71
$BL_{1.7}$	7.8	0.65	0.49	2.5	58	3.22
SL_{PEDOT}	8.6	0.57	0.43	2.1	71	1.73
Optimized	17.5	0.63	0.59	6.5[b]	26	22.41
IL[c] only	3.3	0.024	0.23	0.018	-	-

[a] A 1:1 ratio of lithium ions and *t*BP. [b] A 1.2:1 ratio of lithium ions and *t*BP. Additional photovoltaic performances of different lithium ions and *t*BP ratios are summarized in Table S3. [c] Ionic liquid (EmITFSI).

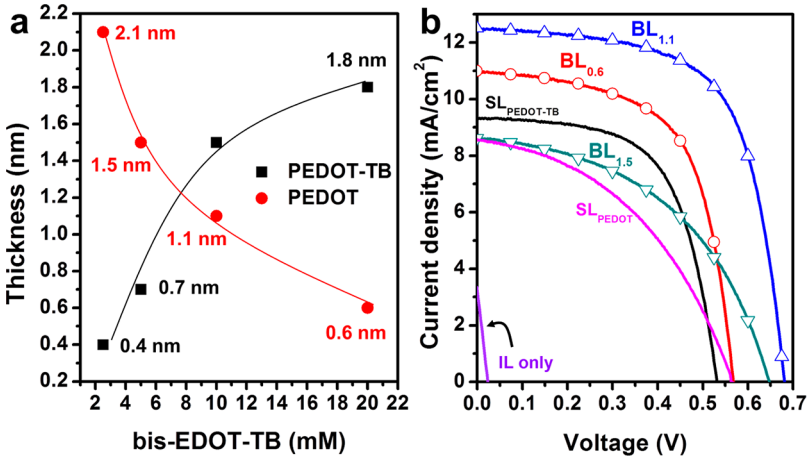

Figure 4. (a) Calculated thicknesses of each polymeric layer as a function of the bis-EDOT-TB concentration. (b) The current density−voltage curves for the single and bilayer sDSCs.

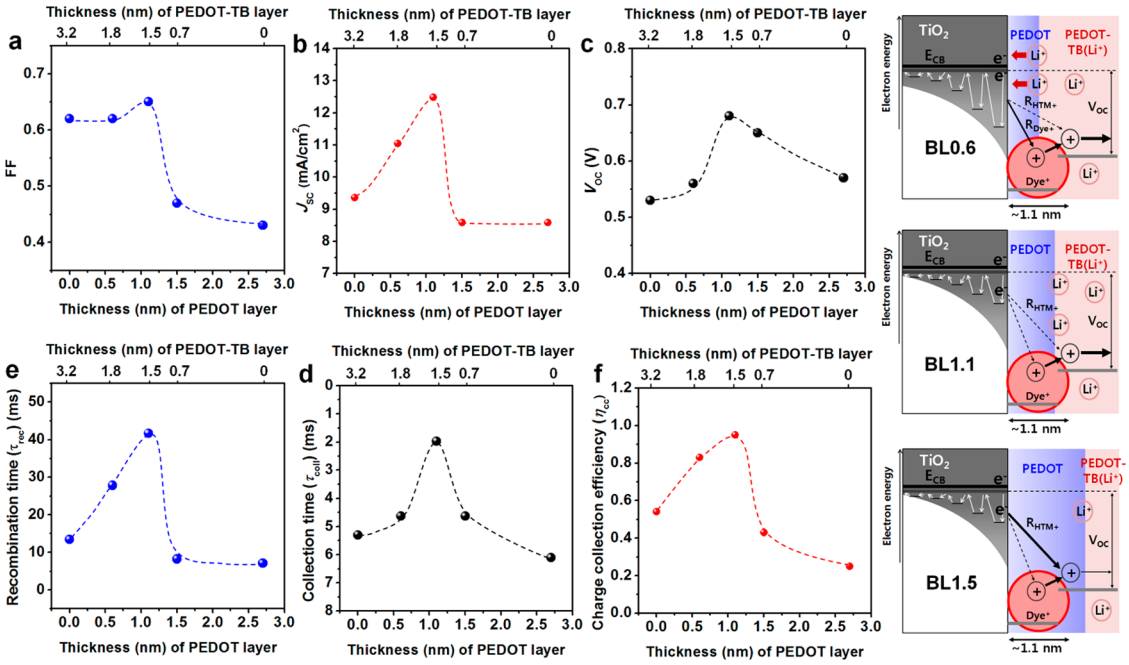

Figure 5. Trends in the photovoltaic parameters and charge transfer/charge transport properties as a function of the PEDOT and PEDOT-TB layer thickness: (a) V_{OC}, (b) FF, (c) J_{SC}, (d) τ_{rec}, (e) τ_{coll}, (f) η_{cc}. Proposed device structures of $BL_{0.6}$, $BL_{1.1}$, and $BL_{1.5}$. See Figure S21 and Table S4 for the reproducibility of the experiments.

polar surface of the TiO_2 particles and to the J_{SC} drop caused by the R_{HTM+}, as reported by Grätzel *et al.*, $V_{OC} \sim (nkT/q) \times \ln(J_{SC}/J_S)$, where, n is the device ideality factor, k is the Boltzmann constant, T is the Kelvin temperature, q is the fundamental charge, and J_S is the saturation current density.[21]

On the other hand, the thickness (1.1 nm) of the PEDOT layer in the $BL_{1.1}$ device was comparable to the size of the sensitizing dye; thus, direct contact between the Dye$^+$ and PEDOT-TB(Li$^+$) layers may increase the J_{SC} and FF values (see the inset ($BL_{1.1}$) in Figure 5). Indeed, the charge collection efficiency ($\eta_{cc} = 1 - \tau_{coll}/\tau_{rec}$)[43] of $BL_{1.1}$ reached values up to 0.95, which is *ca.* 280% improvement compared to SL_{PEDOT}. In addition, the V_{OC} value (0.68 V) was almost identical to the theoretical value (0.68 V), indicating that the low-lying quasi-Fermi levels of the TiO_2 electrode were negligible for a 1.1 nm thick PEDOT blocking layer. Finally, we further optimized $BL_{1.1}$ by varying the concentration of the lithium salts (Table S3 and Figure S20) to obtain a J_{SC} of 17.5, a V_{OC} of 0.63, a FF of 0.59, and a PCE of 6.5%.

CONCLUSIONS

This work describes the first successful synthesis of highly insoluble thiophene-based all-conducting block copolymers (PEDOT-*b*-PEDOT-TBs). We demonstrated the selective positioning of lithium ions on the outer PEDOT-TB layer only. The physical contact between the Dye and the PEDOT-TB(Li$^+$) layers and the ionic contact between the TiO_2 electrode and the Li$^+$ ions on the PEDOT-TB layer were precisely optimized to within 1 nm, yielding extremely effective charge collection (0.25 → 0.95) due to negligible recombination reactions between the photoinduced electrons and the HTM$^+$ and Dye$^+$. Our findings will significantly impact the development of optoelectronic devices and solar cells.

METHODS

Fabrication of sDSCs. TiO_2 compact layer or blocking layer was prepared *via* spin-coating of a solution of 0.25 M titanium(IV) isopropoxide (TIP) in ethanol followed by sintering at 500 °C. Nanoporous TiO_2 electrodes were prepared on a fluorine-doped SnO_2 (FTO) (Pilkington, SnO_2:F, 8 Ω/sq) from the colloidal Nanoxide-T paste (Solaronix) by doctor-blade techniques. The films were annealed at 500 °C for 30 min in air. The resulting TiO_2 films (thickness is around 9 μm, measured by a profiler, α-step 500, KLA Tencor) were cut into pieces. Then, the electrodes were immersed into 0.3 mM *cis*-bis(isothiocyanato)(2,2′-bipyridyl-4,4′-dicarboxylato)(2,2′-bipyridyl-4,4′-dinonyl)ruthenium(II) (known as Z907, Solaronix) in acetonitrile/*tert*-butanol (1:1) for 18 h. *In situ* photoelectrochemical polymerization (PEP) was done by applying constant bias (+0.2 V *vs* Ag/AgCl) (SP-200, Biologic potentiostat) under light irradiation of a 150 W Xe lamp (22 mW cm^{-2}, λ > 520 nm) to the dye-coated TiO_2 for each optimized time. For the PEP, 0.1 M Li-TFSI in acetonitrile was used as an electrolyte which was prepared in advance, and the dye-coated TiO_2 film, platinum foil, and Ag/AgCl was used as a working, a counter, and a reference electrode, respectively. Z907-sensitized working electrode was immersed in each concentration of bis-EDOT-TB solution. A first PEP was performed with bias (+0.2 V *vs* Ag/AgCl) (SP-200, Biologic potentiostat) under light irradiation of a 150 W Xe lamp (22 mW cm^{-2}, λ > 520 nm) in 200 s, and then resulting working electrode was washed with acetonitrile. Second PEP with 0.01 M bis-EDOT monomer solution was processed in 1800 s. After *in situ* PEP, the resulting TiO_2/dye/PEDOT-TB-*b*-PEDOT electrode was rinsed by acetonitrile

and then dried. After that, a drop of EMIm-TFSI with 0.2 M TBP and 0.2 M LiTFSI was added on the surface. For the optimization condition, silver nanowire (60 nm in IPA, sigma Aldrich) was sprayed on the photoanode, and finally the silver paste was painted on them for the fine conductive necking.

Secondary Ion Mass Spectroscopy (SIMS). Samples were prepared by PEP with 0.01 M bis-EDOT-TB and 0.1 M $LiClO_4$ in acetonitrile solution and 0.05 M pyrrole and 0.1 M $LiClO_4$ in acetonitrile solution on Z907-sensitized TiO_2 particles. Elemental mapping of surface and bottom (peeled off) for the resulting bilayered structure was analyzed by the secondary ion mass spectroscopy (SIMS), using a Shimadzu Axima Confidence instrument. O_2^+ gun was used for detection of lithium ions ($_7$Li) with 7.5 keV of beam source. CS^+ gun was used as a beam source (15 keV) and detected ions are nitrogen ($_{14}$N) and sulfur ($_{32}$S).

Solventless MALDI-TOF MS Spectroscopy. Samples were analyzed by the new technique of solventless MALDI, using an Applied Biosystems, Proteomics Analyzer 4700. Intact solar cell films of approximately 1 cm^2 were scraped from their glass backing with a doctor blade. Ten times the mass of 2,5-dihydroxybenzoic acid was added and the contents were mixed with a spatula, then ground with an agate pestle to a fine powder. A small quantity of the powder was picked up on the tip of a fine spatula and smeared well onto the MALDI target. Compressed air was then used to blow any loose material away.

Photoelectrochemical Measurement. A 450 W xenon light source (Model No.94022A, Oriel) was used to apply an illumination power of 100 mW cm^{-2} (the equivalent of one sun at AM1.5) to the surface of the solar cell to simulate solar light irradiation. The incident light intensity was calibrated with reference to a Si solar cell equipped with an IRcutoff filter (KG-5, Schott). Comparison of the simulated light to the true solar spectrum in the region 350−750 nm determined a spectral mismatch of less than 2%. The *I*−*V* characteristics were obtained by measuring the photocurrent generated by the cells (under an applied external bias) using a Keithley model 2400 digital source meter (Keithley). The voltage step and delay time for the measurement were 10 mV and 40 ms, respectively.

Transmission Electron Microscopy (TEM). TEM samples were analyzed by HR-[S]TEM (JEOL JEM-2100F, JEOL) which is 2100F with Cs-corrected STEM. Photoelectrochemically polymerized photoanodes were scraped with a doctor blade and ground with agate pestle to a fine powder. Samples were dispersed in ethanol and one drop of resulting solution was casted on the holey carbon grid (400 mesh).

Raman Spectroscopy. Photoelectrochemically polymerized photoanodes were measured by Raman spectrometer (LABRAM HR800UV, HORIBA JOBIN YVON).

Density Functional Theory (DFT) Calculation. The ground state geometrical structures of Z907 sensitizer were optimized using the DFT with the B3LYP exchange-correlation functional and the 3-21G(d) basis set. The calculation was performed with the GAUSSIAN 09 package.

1D X-ray Diffraction (XRD). The photoanodes coated by PEDOT, PEDOT-TB or PEDOT-*b*-PEDOT-TB as a film were measured in Pohang Accelerator Laboratory (PAL). The accelerator is PLS-II, which has 3.0 GeV beam accelerator with 281.8 m of circumference.

Conflict of Interest: The authors declare no competing financial interest.

Supporting Information Available: PEP mechanism, Raman spectra, 1D XRD spectra, UV−vis spectra, DFT calculation, and photovoltaic performances of DSCs. This material is available free of charge *via* the Internet at http://pubs.acs.org.

Acknowledgment. This work was supported by the Nano. Material Technology Development Program (2012M3A7B4049989), the Center for Advanced Soft Electronics under the Global Frontier Research Program (No. 2011-0031628) and the Basic Science Research Program (No. 2012M1A2A2671699) through a NRF. Experiments at Pohang Accelerator Laboratory were supported in part by MSIP and POSTECH. Partial support for this work was provided by POSCO.

REFERENCES AND NOTES

1. Yella, A.; Lee, H. W.; Tsao, H. N.; Yi, C. Y.; Chandiran, A. K.; Nazeeruddin, M. K.; Diau, E. W. G.; Yeh, C. Y.; Zakeeruddin, S. M.; Gratzel, M. Porphyrin-Sensitized Solar Cells with Cobalt (II/III)-Based Redox Electrolyte Exceed 12% Efficiency. *Science* **2011**, *334*, 629–634.
2. Bach, U.; Lupo, D.; Comte, P.; Moser, J. E.; Weissortel, F.; Salbeck, J.; Spreitzer, H.; Gratzel, M. Solid-state Dye-Sensitized Mesoporous TiO_2 Solar Cells with High Photon-to-Electron Conversion Efficiencies. *Nature* **1998**, *395*, 583–585.
3. Yu, Q. J.; Wang, Y. H.; Yi, Z. H.; Zu, N. N.; Zhang, J.; Zhang, M.; Wang, P. High-Efficiency Dye-Sensitized Solar Cells: The Influence of Lithium Ions on Exciton Dissociation, Charge Recombination, and Surface States. *ACS Nano* **2010**, *4*, 6032–6038.
4. Tian, H. N.; Gabrielsson, E.; Lohse, P. W.; Vlachopoulos, N.; Kloo, L.; Hagfeldt, A.; Sun, L. C. Development of an Organic Redox Couple and Organic Dyes for Aqueous Dye-Sensitized Solar Cells. *Energy Environ. Sci.* **2012**, *5*, 9752–9755.
5. Li, L.; Yang, X. C.; Gao, J. J.; Tian, H. N.; Zhao, J. Z.; Hagfeldt, A.; Sun, L. C. Highly Efficient CdS Quantum Dot-Sensitized Solar Cells Based on a Modified Polysulfide Electrolyte. *J. Am. Chem. Soc.* **2011**, *133*, 8458–8460.
6. Finke, A. D.; Gross, D. E.; Han, A.; Moore, J. S. Engineering Solid-State Morphologies in Carbazole-Ethynylene Macrocycles. *J. Am. Chem. Soc.* **2011**, *133*, 14063–14070.
7. Treat, N. D.; Brady, M. A.; Smith, G.; Toney, M. F.; Kramer, E. J.; Hawker, C. J.; Chabinyc, M. L. Interdiffusion of PCBM and P3HT Reveals Miscibility in a Photovoltaically Active Blend. *Adv. Energy Mater.* **2011**, *1*, 82–89.
8. Clifford, J. N.; Palomares, E.; Nazeeruddin, M. K.; Gratzel, M.; Nelson, J.; Li, X.; Long, N. J.; Durrant, J. R. Molecular Control of Recombination Dynamics in Dye-Sensitized Nanocrystalline TiO_2 Films: Free Energy *vs* Distance Dependence. *J. Am. Chem. Soc.* **2004**, *126*, 5225–5233.
9. Guo, L. J.; Wang, Y. M.; Lu, H. P. Combined Single-Molecule Photon-Stamping Spectroscopy and Femtosecond Transient Absorption Spectroscopy Studies of Interfacial Electron Transfer Dynamics. *J. Am. Chem. Soc.* **2010**, *132*, 1999–2004.
10. Koh, J. K.; Kim, J.; Kim, B.; Kim, J. H.; Kim, E. Highly Efficient, Iodine-Free Dye-Sensitized Solar Cells with Solid-State Synthesis of Conducting Polymers. *Adv. Mater.* **2011**, *23*, 1641–1646.
11. Peter, L. M. Dye-Sensitized Nanocrystalline Solar Cells. *Phys. Chem. Chem. Phys.* **2007**, *9*, 2630–2642.
12. Nelson, J.; Chandler, R. E. Random Walk Models of Charge Transfer and Transport in Dye Sensitized Systems. *Coordin Chem. Rev.* **2004**, *248*, 1181–1194.
13. Furube, A.; Wang, Z. S.; Sunahara, K.; Hara, K.; Katoh, R.; Tachiya, M. Femtosecond Diffuse Reflectance Transient Absorption for Dye-Sensitized Solar Cells under Operational Conditions: Effect of Electrolyte on Electron Injection. *J. Am. Chem. Soc.* **2010**, *132*, 6614–6615.
14. Leventis, H. C.; O'Mahony, F.; Akhtar, J.; Afzaal, M.; O'Brien, P.; Haque, S. A. Transient Optical Studies of Interfacial Charge Transfer at Nanostructured Metal Oxide/PbS Quantum Dot/Organic Hole Conductor Heterojunctions. *J. Am. Chem. Soc.* **2010**, *132*, 2743–2750.
15. Hara, K.; Dan-Oh, Y.; Kasada, C.; Ohga, Y.; Shinpo, A.; Suga, S.; Sayama, K.; Arakawa, H. Effect of Additives on the Photovoltaic Performance of Coumarin-Dye-Sensitized Nanocrystalline TiO_2 Solar Cells. *Langmuir* **2004**, *20*, 4205–4210.
16. Le Bahers, T.; Labat, F.; Pauporte, T.; Ciofini, I. Effect of Solvent and Additives on the Open-Circuit Voltage of ZnO-based Dye-Sensitized Solar Cells: A Combined Theoretical and Experimental Study. *Phys. Chem. Chem. Phys.* **2010**, *12*, 14710–14719.
17. Snaith, H. J.; Moule, A. J.; Klein, C.; Meerholz, K.; Friend, R. H.; Gratzel, M. Efficiency Enhancements in Solid-state Hybrid Solar Cells *via* Reduced Charge Recombination and Increased Light Capture. *Nano Lett.* **2007**, *7*, 3372–3376.
18. Morris, A. J.; Meyer, G. J. TiO_2 Surface Functionalization to Control the Density of States. *J. Phys. Chem. C* **2008**, *112*, 18224–18231.

19. Fabregat-Santiagoa, F.; Bisquert, J.; Palomares, E.; Haque, S. A.; Durrant, J. R. Impedance Spectroscopy Study of Dye-Sensitized Solar Cells with Undoped Spiro-OMeTAD as Hole Conductor. *J. Appl. Phys.* **2006**, *100*, 034510.
20. Boschloo, G.; Haggman, L.; Hagfeldt, A. Quantification of the Effect of 4-*tert*-Butylpyridine Addition to $I^-/I^-_3(-)$ Redox Electrolytes in Dye-Sensitized Nanostructured TiO_2 Solar Cells. *J. Phys. Chem. B* **2006**, *110*, 13144–13150.
21. Nazeeruddin, M. K.; Kay, A.; Rodicio, I.; Humphry-Baker, R.; Mueller, E.; Liska, P.; Vlachopoulos, N.; Graetzel, M. Conversion of Light to Electricity by cis-X2bis(2,2′-Bipyridyl-4,4′-dicarboxylate)ruthenium(II) Charge-Transfer Sensitizers (X = Cl^-, Br^-, I^-, CN^-, and SCN^-) on Nanocrystalline Titanium Dioxide Electrodes. *J. Am. Chem. Soc.* **1993**, *115*, 6382–6390.
22. Nakade, S.; Kanzaki, T.; Kubo, W.; Kitamura, T.; Wada, Y.; Yanagida, S. Role of Electrolytes on Charge Recombination in Dye-Sensitized TiO_2 Solar Cell (1): The Case of Solar Cells Using the $I^-/I_3^-(-)$ Redox Couple. *J. Phys. Chem. B* **2005**, *109*, 3480–3487.
23. Kelly, C. A.; Farzad, F.; Thompson, D. W.; Stipkala, J. M.; Meyer, G. J. Cation-Controlled Interfacial Charge Injection in Sensitized Nanocrystalline TiO_2. *Langmuir* **1999**, *15*, 7047–7054.
24. Jennings, J. R.; Wang, Q. Influence of Lithium Ion Concentration on Electron Injection, Transport, and Recombination in Dye-Sensitized Solar Cells. *J. Phys. Chem. C* **2010**, *114*, 1715–1724.
25. Li, R. Z.; Liu, D. X.; Zhou, D. F.; Shi, Y. S.; Wang, Y. H.; Wang, P. Influence of the Electrolyte Cation in Organic Dye-Sensitized Solar Cells: Lithium *versus* Dimethylimidazolium. *Energy Environ. Sci.* **2010**, *3*, 1765–1772.
26. Abate, A.; Leijtens, T.; Pathak, S.; Teuscher, J.; Avolio, R.; Errico, M. E.; Kirkpatrik, J.; Ball, J. M.; Docampo, P.; McPherson, I.; *et al.* Lithium Salts as "Redox Active" p-Type Dopants for Organic Semiconductors and Their Impact in Solid-state Dye-Sensitized Solar Cells. *Phys. Chem. Chem. Phys.* **2013**, *15*, 2572–2579.
27. Haque, S. A.; Park, T.; Xu, C.; Koops, S.; Schulte, N.; Potter, R. J.; Holmes, A. B.; Durrant, J. R. Interface Engineering for Solid-state Dye-Sensitized Nanocrystalline Solar Cells: The Use of Ion-Solvating Hole-Transporting Polymers. *Adv. Funct. Mater.* **2004**, *14*, 435–440.
28. Xia, J. B.; Masaki, N.; Lira-Cantu, M.; Kim, Y.; Jiang, K. J.; Yanagida, S. Influence of Doped Anions on Poly(3,4-ethylenedioxythiophene) as Hole Conductors for Iodine-free Solid-State Dye-Sensitized Solar Cells. *J. Am. Chem. Soc.* **2008**, *130*, 1258–1263.
29. Song, I. Y.; Park, S. H.; Lim, J.; Kwon, Y. S.; Park, T. A Novel Hole Transport Material for Iodine-Free Solid State Dye-Sensitized Solar Cells. *Chem. Commun.* **2011**, *47*, 10395–10397.
30. Zhang, Y.; Tajima, K.; Hirota, K.; Hashimoto, K. Synthesis of All-Conjugated Diblock Copolymers by Quasi-Living Polymerization and Observation of Their Microphase Separation. *J. Am. Chem. Soc.* **2008**, *130*, 7812–7813.
31. He, M.; Zhao, L.; Wang, J.; Han, W.; Yang, Y. L.; Qiu, F.; Lin, Z. Q. Self-Assembly of All-Conjugated Poly(3-alkylthiophene) Diblock Copolymer Nanostructures from Mixed Selective Solvents. *ACS Nano* **2010**, *4*, 3241–3247.
32. Kim, J.; Song, I. Y.; Park, T. Polymeric Vesicles with a Hydrophobic Interior Formed by a Thiophene-based All-Conjugated Amphiphilic Diblock Copolymer. *Chem. Commun.* **2011**, *47*, 4697–4699.
33. Stefan, M. C.; Javier, A. E.; Osaka, I.; McCullough, R. D. Grignard Metathesis Method (GRIM): Toward a Universal Method for the Synthesis of Conjugated Polymers. *Macromolecules* **2009**, *42*, 30–32.
34. Yokoyama, A.; Kato, A.; Miyakoshi, R.; Yokozawa, T. Precision Synthesis of Poly (N-hexylpyrrole) and Its Diblock Copolymer with Poly(p-phenylene) *via* Catalyst-Transfer Polycondensation. *Macromolecules* **2008**, *41*, 7271–7273.
35. Ng, M. K.; Yu, L. P. Synthesis of Amphiphilic Conjugated Diblock Oligomers as Molecular Diodes. *Angew. Chem., Int. Ed.* **2002**, *41*, 3598–3601.
36. Park, S. J.; Kang, S. G.; Fryd, M.; Saven, J. G.; Park, S. J. Highly Tunable Photoluminescent Properties of Amphiphilic Conjugated Block Copolymers. *J. Am. Chem. Soc.* **2010**, *132*, 9931–9933.
37. Waltman, R. J.; Bargon, J.; Diaz, A. F. Electrochemical studies of some conducting polythiophene films. *J. Phys. Chem.* **1983**, *87*, 1459–1463.
38. Dolan, A. R.; Wood, T. D. Analysis of Polyaniline Oligomers by Laser Desorption Ionization and Solventless MALDI. *J. Am. Soc. Mass. Spectrom.* **2004**, *15*, 893–899.
39. Choi, J.; Park, S. H.; Kwon, Y. S.; Lim, J.; Song, I. Y.; Park, T. Facile Fabrication of Aligned Doubly Open-Ended TiO_2 Nanotubes, *via* a Selective Etching Process, for Use in Front-Illuminated Dye Sensitized Solar Cells. *Chem. Commun.* **2012**, *48*, 8748–8750.
40. Park, S. H.; Lim, J.; Kwon, Y. S.; Song, I. Y.; Choi, J. M.; Song, S.; Park, T. Tunable Nanoporous Network Polymer Nanocomposites having Size-Selective Ion Transfer for Dye-Sensitized Solar Cells. *Adv. Energy Mater.* **2013**, *3*, 184–192.
41. Kwon, Y. S.; Lim, J.; Song, I.; Song, I. Y.; Shin, W. S.; Moon, S. J.; Park, T. Chemical Compatibility between a Hole Conductor and Organic Dye Enhances the Photovoltaic Performance of Solid-State Dye-Sensitized Solar Cells. *J. Mater. Chem.* **2012**, *22*, 8641–8648.
42. Leijtens, T.; Lim, J.; Teuscher, J.; Park, T.; Snaith, H. J. Charge Density Dependent Mobility of Organic Hole-Transporters and Mesoporous TiO_2 Determined by Transient Mobility Spectroscopy: Implications to Dye-Sensitized and Organic Solar Cells. *Adv. Mater.* **2013**, *25*, 3227–3233.
43. Zhu, K.; Neale, N. R.; Miedaner, A.; Frank, A. J. Enhanced Charge-Collection Efficiencies and Light Scattering in Dye-Sensitized Solar Cells Using Oriented TiO_2 Nanotubes Arrays. *Nano Lett.* **2007**, *7*, 69–74.